Journal of Industrial and Engineering Chemistry 96 (2021) 397–403

Contents lists available at ScienceDirect

Journal of Industrial and Engineering Chemistry

journal homepage: www.elsevier.com/locate/jiec

Ultra-fast and efficient calcium co-intercalation host enabled by hierarchically 3D porous carbon nanotemplates

Jin Hwan Kwak[a,b,1], Jong Chan Hyun[c,1], Jae-Ho Park[a,d], Kyung Yoon Chung[a,e], Seung-Ho Yu[b], Young Soo Yun[c,**], Hee-Dae Lim[a,e,*]

[a] Center for Energy Storage Research, Korea Institute of Science and Technology (KIST), Seoul, 02792, Republic of Korea
[b] Department of Chemical and Biological Engineering, Korea University, Seoul, 02841, Republic of Korea
[c] KU-KIST Graduate School of Converging Science and Technology, Korea University, 145 Anam-ro, Seongbuk-gu, Seoul, 02841, Republic of Korea
[d] Department of Materials Science and Engineering, Korea University, Seoul 02841, Republic of Korea
[e] Division of Energy & Environment Technology, KIST School, Korea University of Science and Technology, Seoul 02792, Republic of Korea

ARTICLE INFO

Article history:
Received 26 October 2020
Received in revised form 3 February 2021
Accepted 3 February 2021
Available online 9 February 2021

Keywords:
Ca batteries
Co-intercalation
Crystallinity
Carbonization
Carbon materials
Bacterial cellulose
3D structure

ABSTRACT

As promising candidates for next-generation batteries, calcium-ion batteries (CIBs) have attracted significant attention because of the lower cost and improved environmental friendliness of Ca metal relative to those of Li and their potential to deliver higher energy densities. However, their practical application has been limited by the lack of an appropriate electrode that can induce fast Ca co-intercalation/deintercalation reactions while providing longer cycle life. In this study, we report bacterial cellulose (BC) with a highly graphitic-like ordered structure as a new and efficient co-intercalation host for multivalent Ca ions. The free-standing BC electrode with unique 3D porous morphology possessed ultra-fast co-intercalation kinetics, much faster than that for a commercial graphite electrode. In addition, we addressed the controversial issue of whether Ca co-intercalation truly occurs in the graphitic layer. It is demonstrated that the co-intercalation is directly dependent on the degree of carbon crystallinity by using various BC electrodes with different crystallinities at regular intervals. Finally, the effect of the ordering of the carbon stacking layer on the co-intercalation chemistry was electrochemically investigated.

Introduction

The rapid development of energy storage systems (ESSs) from portable devices to large-scale devices such as drones and electric vehicles has motivated the development of next-generation batteries [1–4]. In addition, significant concerns about the depletion of fossil fuels and global environmental issues have guided numerous researchers to focus on developing renewable energies and efficient ESSs [5,6]. Until now, Li-ion batteries (LIBs) have occupied most of the battery market share because of their high power and energy densities and long-term cycle life [7–9]. However, the limited Li metal sources and expensive cell components used for fabricating LIBs have raised concerns; therefore, exploring a substitutional charge carrier instead of Li ion with abundant and ubiquitous elements is crucial for the advancement of next-generation batteries.

Among the many potential candidates for next-generation batteries, calcium-ion batteries (CIBs) have been highlighted as an ideal substitution for LIBs because of the abundance of calcium metal in the Earth's crust as well as its relatively low cost [10,11]. Multivalent calcium ions can theoretically provide two electrons per ion during redox reactions and have a substantially low redox potential of –2.87 V (*vs.* standard hydrogen electrode), indicating the great potential for the realization of high-energy-density CIBs [12–14]. Moreover, the electrochemical kinetics of calcium ions has been reported to be faster than that of other multivalent ions because of their relatively low polarizability [15,16]. In the field of CIBs, attention has thus far mostly been focused on identifying an appropriate electrolyte because the critical issues are mainly related to the electrolyte and its compatibility with Ca metal [10,17–20]. Relatively fewer studies have aimed to identify an appropriate electrode material as a host for accommodating Ca ions [21,22]. However, considering that conventional layered-type

* Corresponding author at: Center for Energy Storage Research, Korea Institute of Science and Technology (KIST), Seoul 02792, Republic of Korea.
** Corresponding author.
E-mail addresses: c-ysyun@korea.ac.kr (Y.S. Yun), hdlim@kist.re.kr (H.-D. Lim).
[1] These authors contributed equally to this work.

https://doi.org/10.1016/j.jiec.2021.02.006
1226-086X/

materials hardly accommodate multivalent Ca ions because of the strong ionic interactions of multivalent ions, it is crucial to explore new intercalation materials to enable the realization of high-energy-density CIBs [23–26].

It has recently been reported that multivalent Ca ions can be readily co-intercalated into graphite by combining with electrolyte molecules. The complexes of Ca ions and electrolyte molecules are known to intercalate into graphite layers because of the shielding effect of electrolytes. The multivalent Ca ions surrounded by electrolyte molecules can alleviate the strong ionic interaction of the cations, enabling Ca co-intercalation with acceptable reversible capacities of approximately 85 mA h g^{-1} [27]. However, two major issues must be solved to advance the co-intercalation chemistries in the field of CIBs. (1) There are controversial opinions on whether Ca co-intercalation really occurs; thus, reliable proof must be provided. (2) The kinetics of co-intercalation must be enhanced because the heavy ion complexes are entangled together; thus, their motions are inevitably sluggish. Designing an efficient host for Ca co-intercalation is the key to achieving fast kinetics for CIBs.

In this study, to overcome these two major issues, we fabricated a three-dimensional (3D) porous carbon electrode based on bacterial cellulose (BC). The graphitized carbon host of BC was chosen because it has a graphitic-like ordered nanostructure with numerous pores, which is advantageous to provide electrical conducting routes as well as fast ion pathways [28–30]. By systematically controlling the heat-treatment conditions, BC electrodes with different crystallinities were prepared. The BC electrodes were electrochemically tested to investigate the effect of carbon crystallinity on the Ca co-intercalation ability. The more graphitized electrodes resulted in higher capacities, implying that co-intercalation is directly dependent on the degree of carbon crystallinity. Furthermore, it was demonstrated that the unique structure of BC-derived carbon materials (*i.e.*, 3D nanoweb structures) provide facile access to heavy Ca ion and electrolyte complexes, leading to an ultra-fast rate capability. The BC electrodes exhibited markedly faster kinetics than commercial graphite, indicating that the use of a BC electrode with 3D nanoweb structures is a promising route to achieving high-rate CIBs. While the porous host of BC has been utilized in the fields of LIBs [31–33], it is a first demonstration for BC to efficiently host co-intercalation materials in CIBs.

Experimental

Preparation of BC-derived carbon materials

BC hydrogels were prepared using *Acetobacter xylinum* BRC 5 in Hestrin and Schramm medium using a previously reported method [34]. To exchange the solvents, the BC hydrogels were immersed in tert-butanol. The BCs were then freeze-dried at −45 °C for 72 h, producing a white-colored cryogel. To prepare various BC carbons with systematically different crystallinities, each carbonization step was performed at six different temperatures of 800 °C, 1200 °C, 1600 °C, 2000 °C, 2400 °C, and 2800 °C in a graphitization furnace (ThermVac, South Korea). The regular intervals of the temperatures were reached at the systematically controlled heating rates of 10 °C min^{-1} from 25 °C to 1800 °C, 5 °C min^{-1} from 1800 °C to 2400 °C, and 3 °C min^{-1} from 2400 °C to 2800 °C under an Ar flow rate of 200 mL min^{-1}. After the graphitization, all the samples were treated with a fresh air at 400 °C for 2 h, then the final products were obtained after cooling down to 25 °C.

Characterization

The morphology and microstructure of the BC-derived carbon materials were examined using field-emission scanning electron microscopy (FE-SEM, S-4300SE, Hitachi, Japan) and field-emission transmission electron microscopy (FE-TEM, JEM2100F, JEOL, Japan). X-ray diffraction (XRD, Rigaku DMAX 2500) analysis was performed using Cu-K_α radiation (λ = 0.154 nm) at 40 kV and 100 mA. The Raman spectra for the BC-derived carbon materials were obtained using a continuous linearly polarized laser with a wavelength of 532 nm and a 1200 groove mm^{-1} grating. The spot diameter of the Raman laser was approximately 1 nm, and a 100× objective lens was used. The chemical bonding of the samples was characterized using X-ray photoelectron spectroscopy (XPS, PHI 5700 ESCA, USA) with monochromatic Al K_α radiation ($h\nu$ = 1,486.6 eV).

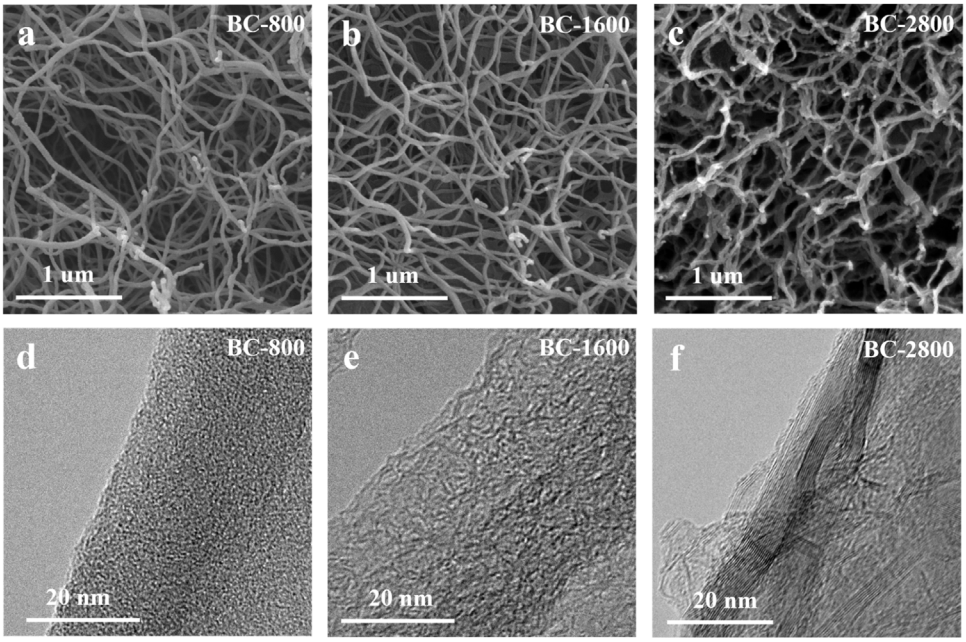

Fig. 1. SEM and TEM images of BC electrodes with different crystallinities. FE-SEM images of (a) BC-800, (b) BC-1600, and (c) BC-2800. FE-TEM images of (d) BC-800, (e) BC-1600, and (f) BC-2800.

Electrochemical characterization

The BC-derived carbon materials were used as free-standing electrodes without further treatment. The diameter and mass of the electrodes were 0.72 cm^2 and ~1.0 mg, respectively. The electrolyte was prepared by dissolving 0.5 M $Ca(BH_4)_2$ in dimethylacetamide (DMAc). Before use, the salt was dried in a vacuum oven set to 150 °C, and the solvent was purified using a molecular sieve. A graphite anode was prepared by mixing graphite powder (Hitachi, SMG A-5, active material, 80 wt.%), Super P (conduct agent, 10 wt.%), and polyvinylidene fluoride (PVDF, binder, 10 wt.%) with *N*-methyl-2-pyrroloidone. The slurry was cast on Cu foil with a thickness of 50 μm, and the active material was loaded with a similar mass as the BC carbon materials (~1.0 mg). To evaporate the solvent, the cast electrode was heated in a convection oven set to 80 °C for 6 h. The electrochemical tests were performed using 2032-type coin cells with a glass microfiber filter (GF/F, Whatman) as the separator. Calcium metal foil was used as the reference/counter electrode after stripping off its surface to remove the passivation layers. All the cells were assembled in an Ar-filled glove box, where the oxygen and water concentrations were maintained below 0.1 ppm.

Results and discussion

To investigate whether Ca co-intercalation truly occurs in the graphitized carbon host, various BC electrodes with different crystallinities were prepared by systematically controlling the heat-treatment temperatures from 800 °C to 2800 °C (Fig. 1). We intentionally designed the BC electrodes to have different crystallinities at a regular gradient while maintaining similar macrostructures. Thus, the prepared BC electrodes could be used to investigate the relationship between the co-intercalation ability and the crystallinity of the carbon host. The morphologies of the prepared BC electrodes were examined using FE-SEM and FE-TEM, as shown in Fig. 1. Regardless of the heat-treatment temperature, all the electrodes exhibited porous and 3D nanoweb structures (Fig. 1a–c); however, their crystalline features varied, as observed in the TEM images (Fig. 1d–f). The crystallinity and degree of stacking of each BC electrode gradually increased with increasing

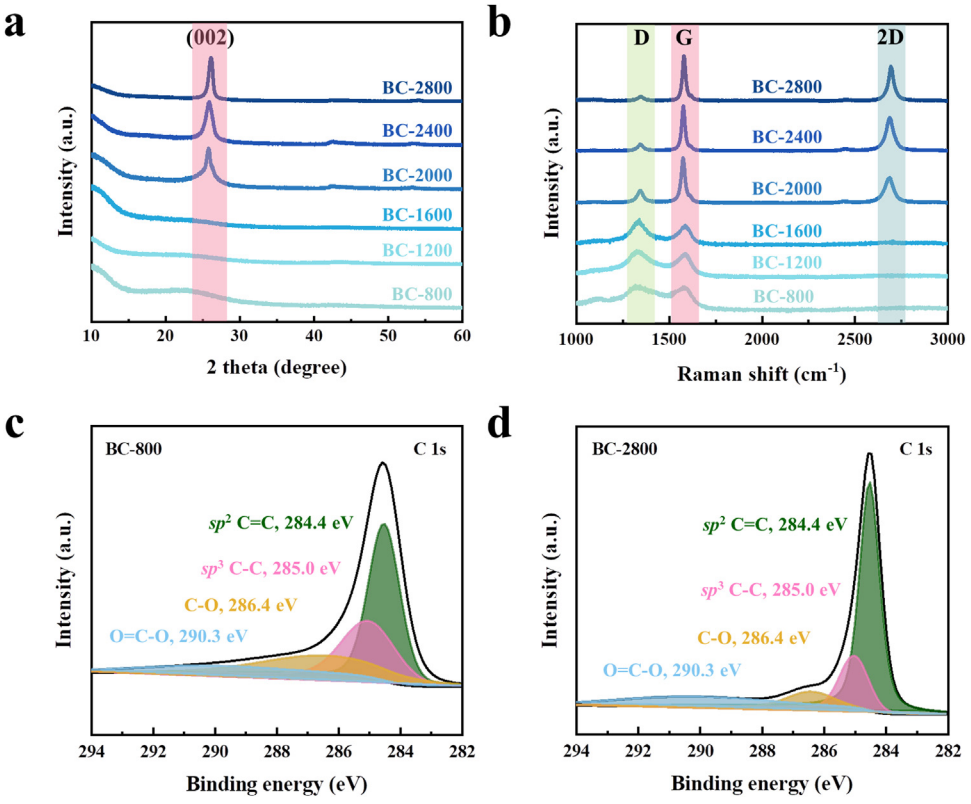

	Atomic ratio (%)[a]		
Samples	C	N	O
BC-800	85.28	0.92	13.80
BC-1200	95.67	0.77	3.56
BC-1600	96.10	0.81	3.07
BC-2000	98.41	0.40	1.19
BC-2400	98.53	0.33	1.15
BC-2800	98.28	0.65	1.07

[a] data from XPS

Fig. 2. Characterization of microstructures and chemical properties of BC electrodes: (a) XRD pattern and (b) Raman spectra of BC electrodes. XPS C 1s spectra of (c) BC-800 and (d) BC-2800.

carbonization temperature (Fig. 1d–f). Detailed comparisons of all the BC electrodes (BC-800, BC-1200, BC-1600, BC-2000, BC-2400, and BC-2800) are provided in Fig. S1. Carbon materials are generally composed of manifold basic structural units (BSUs), and the sizes of the BSUs increased with increasing heating temperature from 800 °C to 2800 °C. In other words, carbonization at higher temperature resulted in a higher degree of graphitization. BC-800 had an amorphous carbon structure with short-range carbon ordering, whereas BC-2800 had a crystalline structure with long-range carbon ordering. In addition, the stacking layers of sp^2 carbon were especially dominant with heat treatment above 2000 °C (*i.e.*, BC-2000, BC-2400, and BC-2800).

For more in-depth analysis of their microstructures, further characterization was performed using XRD, Raman, and XPS. As observed in the XRD patterns (Fig. 2a), sharp (002) peaks dominated at the BC-2000, BC-2400, and BC-2800 samples, whereas the characteristic (002) peak did not appear for the BC-800, BC-1200, and BC-1600 samples. As the graphite (002) peak is a simple index that measures the degree of carbon layer stacking [35], it was concluded that the degree of graphitization was more developed with increasing target temperature. Furthermore, the graphite-like structures were clearly dominant for the BC electrodes heat-treated above 2000 °C; in contrast, those heat-treated under 2000 °C showed no characteristic peaks. *d*-spacing (*d*) of BC-electrode was calculated by using Bragg's law equation ($n\lambda = 2d\sin\theta$, where n is a positive integer, λ is the wavelength, and θ is a degree). The calculated *d*-values of BC-2000, −2400, and −2800 are corresponding to 0.34235, 0.34124, and 0.33775 Å. As the target temperature increases, *d*-values are narrowed, which means that the graphitization of BC electrode is well processed. This phenomenon was again demonstrated in the Raman spectra (Fig. 2b). The G band (centered at 1580 cm^{-1}) and 2D band (centered at 2700 cm^{-1}), which are measures of the degree of hexagonal carbon rings and carbon layer stacking [36], respectively, increased with increasing heat-treatment temperature. The sharp G and 2D bands were more obvious for BC-2000, BC-2400, and BC-2800, as similarly demonstrated by tracing the (002) peaks of Fig. 2a. Furthermore, the D band (1350 cm^{-1}), as a measure of the degree of disordered hexagonal carbon rings, was greatly diminished for heat-treatment above 2000 °C. Therefore, the XRD data and Raman spectra are consistent, demonstrating that the stacking layers with ordered hexagonal carbon rings were more arranged with increasing carbonization temperature.

The surface property of each BC electrode was closely examined using XPS (Fig. 2c and d). Here, we focus on comparing the two extremes of BC-800 and BC-2800, as shown in Fig. 2c and d. XPS data for the all the BC electrodes are also provided in Fig. S2. The intensities of sp^2 C=C bonding of the BC carbons gradually increased with increasing carbonization temperature, as simply confirmed by comparing the height of C=C bonding of each BC electrode (Fig. S2). As observed in Fig. 2c and d, the clear dominant sp^2 bonding in BC-2800 indicates that BC-2800 is much more graphitized than BC-800. Furthermore, as observed in Fig. 2e, the amount of oxygen functional groups gradually changed depending on the heat-treatment temperature. The smallest atomic percentage of oxygen functional groups was measured for BC-2800, whereas a value almost thirteen times higher was detected for BC-800. In short, various BC electrodes with different crystallinities at regular intervals were well prepared while their micro 3D porous structures were similarly maintained. Based on their characteristic properties, they could be divided into two distinct groups: low-crystal BC-derived samples (LCBC; BC-800, BC-1200, and BC-1600) and high-crystal BC-derived samples (HCBC; BC-2000, BC-2400, and BC-2800).

To understand how the different carbon crystallinities affected the Ca co-intercalation chemistries, electrochemical tests were performed for the two groups, as shown in Fig. 3. The prepared BC electrodes were used as free-standing working electrodes, and calcium metal was used as the counter/reference electrode. The electrolyte of 0.5 M $Ca(BH_4)_2$ in *N*,*N*-dimethylacetamide (DMAc) was used because it has been reported to trigger Ca co-intercalation into graphite [27]. Galvanostatic charge/discharge (GC/GDC) tests were performed at various current densities ranging from 50 to 2000 mA g^{-1}, as shown in Figs. 3 and S3. The GC/GDC profiles of LCBC consist of only sloppy shapes with negligible capacities, which may have originated from minor capacitive reactions (Fig. 3a–c). However, the GC/GDC profiles of the HCBCs (Fig. 3d–f) present several plateaus, suggesting the active two-phase reactions (*i.e.,* faradaic reactions). The voltage profiles are well matched to those of a previous paper mentioning Ca co-intercalation reactions [27]. As the two-phase reaction is direct evidence of the Ca co-intercalation, it is clear that the Ca storage behavior is highly affected by the crystallinity of the carbon host. More importantly, the co-intercalation ability is proportional to the degree of carbon crystallinity, indicating that the graphitized feature of carbon allows efficient Ca co-interactions.

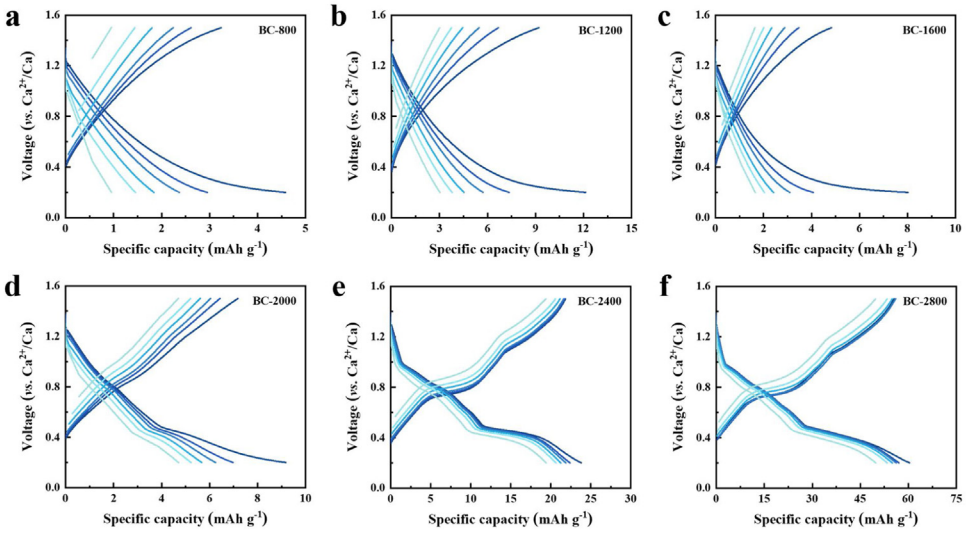

Fig. 3. Galvanostatic charge/discharge profiles of BC-derived samples at current densities of 50, 100, 200, 500, 1000, and 2000 mA g^{-1}: (a) BC-800, (b) BC-1200, (c) BC-1600, (d) BC-2000, (e) BC-2400, and (f) BC-2800.

To electrochemically determine whether a diffusion-controlled reaction truly occurs in BC-2800, cyclic voltammograms (CVs) were obtained at various scan rates ranging from 0.025 to 1.0 mV s^{-1} (Fig. 4a). Four anodic peaks and three cathodic peaks corresponding to intercalation and de-intercalation of Ca ions, respectively, were identified, and each peak was marked by a number 1–7 (indicated by different colored stars in Fig. 4). The kinetics of Ca co-intercalation into BC-2800 at each two-phase reaction were elucidated by calculating the *b*-value obtained from the CV data based on a relationship (1) of $i = av^b$, where *i*, *a*, and *v* are the peak current, constant, and scan rate, respectively (Fig. 4b, c) [37]. The *b*-value is a parameter that measures the degree of dependence on capacitive ($b = 1$; *v*) or diffusion reaction ($b = 0.5$; $v^{1/2}$). In the case of intercalation, the *b*-value of peak 4 was lowest, which means that the active redox at approximately 0.3 V was relatively more affected by diffusion-controlled behaviors than that at peaks 1, 2, and 3 (Fig. 4b). Similarly, the b-value of peak 5 at 0.82 V was lowest during de-intercalation (Fig. 4c). In addition, to trace where the diffusion-controlled reaction had an effect during the charge process, the formulation (2) of $i = k_1 v + k_2 v^{1/2}$ (Fig. 4d, e) was used because k_1 and k_2 are clear indicators that can be used to distinguish capacitive- and diffusion-controlled regions, respectively [38]. The calculated k_2 values of peak 4 and 5 were higher than those of the others, indicating that the reactions occurring at peak 4 and 5 were more affected by the diffusion than the others. In addition, the higher values of k_1 compared with k_2 indicate that capacitive reactions were also included. The results suggest that the combinations of capacitive- and diffusion-controlled reactions contribute to the fast kinetics of BC-2800; however, further study is needed to fundamentally understand this phenomenon. Furthermore, the diffusivity during Ca co-intercalation can be determined using the Randles–Sevcik equation (3), $i_p = 2.69 \times 10^5 n^{3/2} A D^{1/2} C v^{1/2}$, at room temperature, where *n*, *A*, *D*, and *C* denote the number of electrons, area of the electrodes, diffusion coefficient, and concentration of Ca^{2+}, respectively [39]. In this equation, when the peak current (*i*) is linearly related to the square root of scan rate (*v*) for any reaction, the reaction is considered to be affected by diffusion-controlled behavior. In Fig. 4f, all the peaks have linear profiles, and in particular, peak 4 and 5 have the higher absolute values of the slopes, indicating the fast diffusion properties in the regions of peak 4 and 5.

It is worth mentioning that the unique structure of BC-2800 is advantageous to enabling the fast transport of heavy ion complexes (*i.e.*, Ca ion and electrolyte molecules), resulting in improved co-intercalation capability. As already demonstrated in Fig. 3f, the half-cell with BC-2800 delivered a charge capacity of 54 mA h g^{-1} at a current density of 50 mA g^{-1} (Fig. 3f), and surprisingly, most of the capacity was maintained (48 mA h g^{-1}) even at the extremely high current rate of 2000 mA g^{-1}. This result was observed because the unique 3D porous nanoweb structure of BC ensures facile access of bulk ion complexes, as schematically illustrated in Fig. 5a. Naturally, the density of BC electrode is relatively low about 0.09 g cm^{-3} compared to the normal electrodes used in LIBs [40–42]. The macroporous graphitic structure helps to expose carbon nanotubes to the electrolyte; therefore, most surfaces of graphitized carbons could be activated, resulting in wide windows where the ion complexes efficiently co-intercalated. In other words, graphitized free-standing BC electrodes ensure the facile and fast access of Ca ions through the 3D nanoweb structure, resulting in improved rate capability. The rate capabilities are comparable to the previous outstanding results using various carbon-based materials as indicated in Table S1. In addition, a specific capacity can be improved because BC-2800s is a free-standing electrode (Fig. 5b), which doesn't require heavy current collects such as Cu and Al. In Fig. 5c, the capacity retention of the BC-2800 electrode is compared with that of commercial graphite as it has been reported to well-accommodate Ca-ion complexes [26]. At relatively low current rates, their capacity retentions appear to be similar; however, BC-2800 shows superior capacity retention ability at the high current density of 2000 mA g^{-1}. It is reasonable that it is difficult to achieve a high rate capability using commercial graphite because its intrinsic morphology of a 2D structure has limited active edges where Ca-ion complexes can be intercalated. In contrast, the 3D structure of BC-2800 facilitates the fast access of Ca ions to active edge sites of the stacking layers from every direction, thereby showing the high capacity retention even at the extremely high current density of 2000 mA g^{-1}. In addition, the structural stability of BC-2800 was compared with that of the graphite electrode in a cyclability test, as shown in Fig. 5d. Whereas the graphite electrode showed fast decay of the capacity retention and sudden death after ~100 cycles, BC-2800 sustained a high capacity retention of 75% after

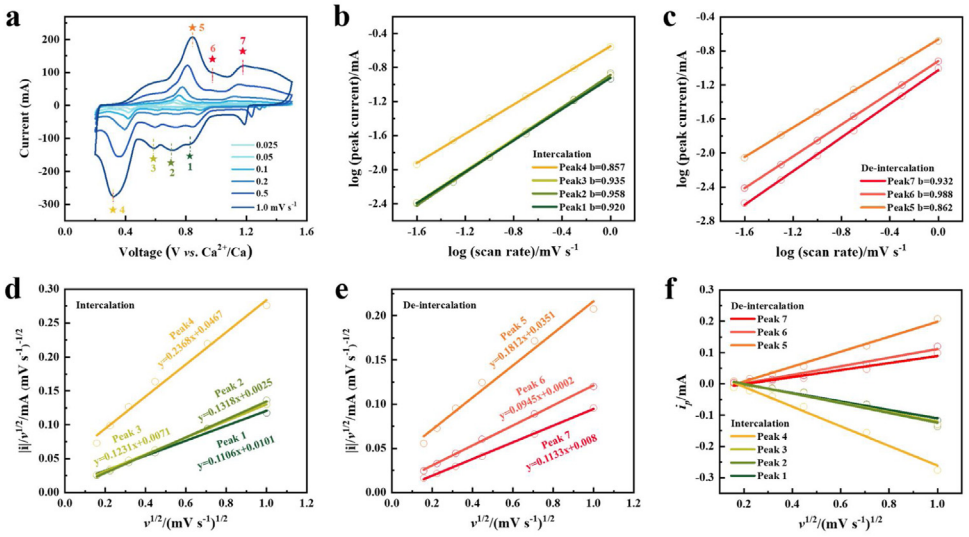

Fig. 4. Analysis on kinetics of Ca storage behaviors on BC-2800. (a) Cyclic voltammograms of BC-2800 at various scan rates from 0.025 to 1.0 mV s^{-1}. Calculation of *b*-value during (b) intercalation and (c) de-intercalation. The current dependency when Ca-ions were (d) intercalated and (e) de-intercalated. (f) The high slope value means the high diffusion coefficient according to Randles-Sevcik equation.

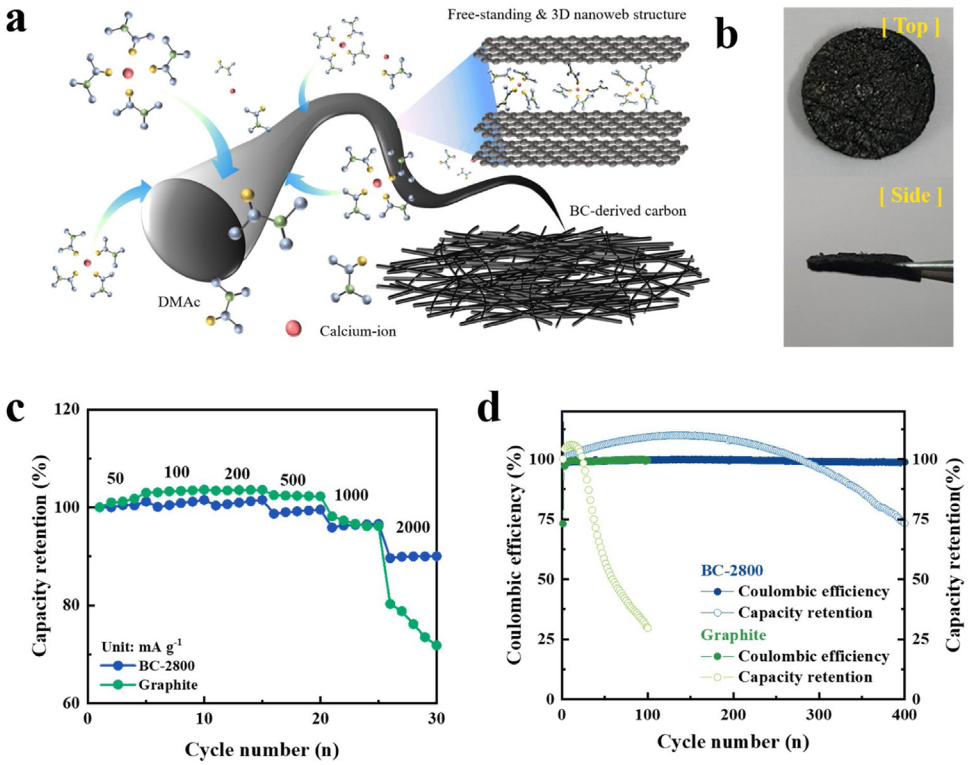

Fig. 5. (a) A schematic image of 3D BC electrode in 0.5 M $Ca(BH_4)_2$ in DMAc electrolyte. (b) Optical images of BC-2800. (c) Rate capability tests at various current densities with 5 cycles of BC-2800 and graphite. (d) Rate capability tests without limitation of cycle at various current densities from 50 to 2000 mA g^{-1} of BC-2800 and graphite.

400 cycles with almost 100% coulombic efficiency. This result is attributed to the highly opened 3D structure of BC-2800 composed of well-graphitized carbon stacking layers, which not only improved the rate capability for the co-intercalation reaction but also enhanced the structural stability with longer cycle life.

Conclusion

In summary, we provided insight on Ca co-intercalation into graphitized carbon stacking layers by performing electrochemical tests of BC electrodes fabricated using bacterial cellulose. By systematically controlling their heat-treatment temperatures, various BC electrodes with different crystallinities at regular intervals were prepared. The effect of carbon crystallinity on the degree of co-intercalation was then electrochemically investigated. We concluded that the capacity delivered by the co-intercalation reaction is directly dependent on the degree of carbon stacking layers. In addition, we designed the unique morphology of a BC electrode with porous 3D nanoweb structures to achieve the optimal condition for co-intercalation of Ca ions into carbon layers. The facile access of ion complexes resulted in ultra-fast rate capability even with high stability over 400 cycles, which is much improved performance compared with that of commercial graphite electrodes. These results demonstrate that the porous BC electrode with nanoweb structure is a promising architecture, potentially beyond current graphite electrodes, and our research will open up new research paths for co-intercalation-based CIBs.

Declaration of interests

The authors declare that they have no known competing financial interests or personal relationships that could have appeared to influence the work reported in this paper.

Acknowledgments

This research was supported by KIST Institutional Program (No. 2E30991) and supported by the Development Program of Core Industrial Technology (No. 20012318) funded by the Ministry of Trade, Industry and Energy of Korea; the Technology Development Program to Solve Climate Changes of the National Research Foundation (NRF), funded by the Ministry of Science & ICT of Korea (2017M1A2A2044482).

Appendix A. Supplementary data

Supplementary material related to this article can be found, in the online version, at doi:https://doi.org/10.1016/j.jiec.2021.02.006.

References

[1] A.S. Arico, P. Bruce, B. Scrosati, J.-M. Tarascon, W. Van Schalkwijk, Nat. Mater. 4 (2005) 366.
[2] M. Armand, J.-M. Tarascon, Nature 451 (2008) 652.
[3] P. Simon, Y. Gogotsi, Nat. Mater. 7 (2008) 845.
[4] B. Dunn, H. Kamath, J.-M. Tarascon, Science 334 (2011) 928.
[5] P. Alotto, M. Guarnieri, F. Moro, Renew. Sustain. Energy Rev. 29 (2014) 325.
[6] C. Liu, F. Li, L.P. Ma, H.M. Cheng, Adv. Mater. 22 (2010) E28.
[7] J.B. Goodenough, Y. Kim, Chem. Mater. 22 (2010) 587.
[8] V. Etacheri, R. Marom, R. Elazari, G. Salitra, D. Aurbach, Energy Environ. Sci. 4 (2011) 3243.
[9] N. Nitta, F.X. Wu, J.T. Lee, G. Yushin, Mater. Today 18 (2015) 252.
[10] M. Wang, C. Jiang, S. Zhang, X. Song, Y. Tang, H.-M. Cheng, Nat. Chem. 10 (2018) 667.
[11] J. Muldoon, C.B. Bucur, T. Gregory, Chem. Rev. 114 (2014) 11683.
[12] D. Wang, X. Gao, Y. Chen, L. Jin, C. Kuss, P.G. Bruce, Nat. Mater. 17 (2018) 16.
[13] D. Larcher, J.-M. Tarascon, Nat. Chem. 7 (2015) 19.
[14] A.L. Lipson, B.F. Pan, S.H. Lapidus, C. Liao, J.T. Vaughey, B.J. Ingram, Chem. Mater. 27 (2015) 8442.
[15] A. Ponrouch, C. Frontera, F. Bardé, M.R. Palacín, Nat. Mater. 15 (2016) 169.
[16] A. Ponrouch, M.R. Palacín, Curr. Opin. Electrochem. 9 (2018) 1.
[17] D. Aurbach, R. Skaletsky, Y. Gofer, J. Electrochem. Soc. 138 (1991) 3536.

[18] Z. Li, O. Fuhr, M. Fichtner, Z. Zhao-Karger, Energy Environ. Sci. 12 (2019) 3496.
[19] S. Biria, S. Pathreeker, H. Li, I.D. Hosein, ACS Appl. Energy Mater. 2 (2019) 7738.
[20] K.V. Nielson, J. Luo, T.L. Liu, Batteries Supercaps 3 (2020) 1.
[21] S. Wu, F. Zhang, Y. Tang, Adv. Sci. 5 (2018)1701082.
[22] Z. Yao, V.I. Hegde, A. Aspuru-Guzik, C. Wolverton, Adv. Energy Mater. 9 (2019) 1802994.
[23] R.J. Gummow, G. Vamvounis, M.B. Kannan, Y. He, Adv. Mater. 30 (2018) 1801702.
[24] M.E. Arroyo-de Dompablo, A. Ponrouch, P. Johansson, M.R. Palacín, Chem. Rev. 120 (2020) 6331.
[25] S.J. Richard Prabakar, A.B. Ikhe, W.B. Park, K.C. Chung, H. Park, K.J. Kim, D. Ahn, J. S. Kwak, K.S. Sohn, M. Pyo, Adv. Sci. 6 (2019)1902129.
[26] S.J. Richard Prabakar, K.-S. Sohn, M. Pyo, ACS Appl. Mater. Interfaces 12 (2020) 16481.
[27] J. Park, Z.-L. Xu, G. Yoon, S.K. Park, J. Wang, H. Hyun, H. Park, J. Lim, Y.-J. Ko, Y.S. Yun, K. Kang, Adv. Mater. 32 (2020)1904411.
[28] S. Deng, Y. Zhang, D. Xie, L. Yang, G. Wang, X.S. Zheng, J. Zhu, X. Wang, Y. Yu, G. Pan, X. Xia, J. Tu, Nano Energy 58 (2019) 355.
[29] S. Jiao, A. Zhou, M. Wu, H. Hu, Adv. Sci. 6 (2019)190025.
[30] X. Liu, H. Xu, H. Ji, K. Zhang, D. Wang, Appl. Surf. Sci. 530 (2020)147261.
[31] B. Wang, X. Li, B. Luo, J. Yang, X. Wang, Q. Song, S. Chen, L. Zhi, Small 9 (2013) 2399.
[32] H.-D. Lim, Y.S. Yun, Y. Ko, Y. Bae, M.Y. Song, H.J. Yoon, K. Kang, H.-J. Jin, Carbon 118 (2017) 114.
[33] M. Lee, Y. Yoo, J.H. Kwak, Y.S. Yun, H.-G. Jung, D. Byun, S.H. Oh, H.-D. Lim, Chem. Eng. J. 412 (2021)128549.
[34] Y.S. Yun, H. Bak, H.-J. Jin, Synth. Met. 160 (2010) 561.
[35] Z.Q. Li, C.J. Lu, Z.P. Xia, Y. Zhou, Z. Luo, Carbon 45 (2007) 1686.
[36] L.G. Cancado, K. Takai, T. Enoki, M. Endo, Y.A. Kim, H. Mizusaki, A. Jorio, N.L. Speziali, M.A. Pimenta, Carbon 46 (2008) 272.
[37] J. Wang, J. Polleux, J. Lim, B. Dunn, J. Phys. Chem. C 111 (2007) 14925.
[38] T. Liu, Z. Zhou, Y. Guo, D. Guo, G. Liu, Nat. Commun. 10 (2019) 1.
[39] D. Cao, C. Yin, D. Shi, Z. Fu, J. Zhang, C. Li, Adv. Funct. Mater. 27 (2017)1701130.
[40] R. Moshtev, B. Johnson, J. Power Sources 91 (2000) 86.
[41] F. Hennrich, S. Lebedkin, S. Malik, J. Tracy, M. Barczewski, H. Rösner, M. Kappes, Phys. Chem. Chem. Phys. 4 (2002) 2273.
[42] C. Kang, M. Patel, B. Rangasamy, K.-N. Jung, C. Xia, S. Shi, W. Choi, J. Power Sources 299 (2015) 465.